2. 1. 4. 3 Simulation from the DTL to the ACS

Some results of simulations from the DTL to the ACS are presented. Five kinds of error simulations were performed:

type-1: normal simulation without introducing any errors,

type-2: random errors in an accelerating field of ±1% in both cells and tanks, random rf phase errors of ±1% in cells and ±3% in tanks and random errors in the transverse position of the focusing magnets of ±0.05 mm,

type-3: increases in the transverse beam sizes of 10% at the DTL entrance in addition to type-2,

type-4: increases in the transverse beam sizes of 20% at the DTL entrance in addition to type-2,

type-5: random large errors in the transverse position of the focusing magnet along the ACS up to ±1 mm in addition to type-2.

The simulations were performed by using a modified PARMILA code with 30000 particles initially distributed in a waterbag. A peak current of 50 mA was assumed.

Table 2.1.4.3.1 summarizes the output normalized emittances. Figure 2.1.4.3.1 show the output emittances for both type-1 and 3 simulations. Figure 2.1.4.3.2 shows the fraction of output particles in x-y space for type-1 to 4 simulations. It can be seen that the injection errors in the beam sizes cause halo-like particles of order of 10^{-4} around the core part. Therefore, accurate tuning of the injection parameters at each transition point should be emphasized. One of the effective tuning methods is to measure nearly full emittances or to measure a fraction of the halo-like part of the beam after some acceleration.

The errors in the transverse position of the focusing magnets (type-5 simulation) cause large transverse oscillation and beam losses in the high-energy region as well as emittance growth. Figure 2.1.4.3.3 shows the transmission ratio as a function of the random position errors in the focusing magnets. Figure 2.1.4.3.4 shows the output transverse emittances in the type-5 simulation. Figure 2.1.4.3.5 shows the average beam position along the ACS for random errors of ±0.05 and ±0.5 mm, respectively. Judging from the above-

Table 2.1.4.3.1 Calculated ACS output emittances for four kinds of simulations.

	x-x' π-mm-mrad		y-y' π -mm-mrad		Δϕ–Δw π -MeV-deg	
	rms	99.9%	rms	99.9%	rms	99.9%
input at 3 MeV	0.200	1.44	0.198	1.43	0.140	1.00
type-1	0.236	3.69	0.231	3.07	0.623	10.9
type-2	0.242	3.80	0.242	3.49	0.672	10.9
type-3	0.311	7.35	0.307	8.31	0.635	9.77
type-4	0.341	8.22	0.336	9.52	0.669	9.33

mentioned results, both a precise beam-position monitor system and some sets of steering magnets in addition to an accurate alignment of the focusing magnets are important to keep the average beam position at less than a limited value, which can be specified according to the allowable emittance growth.

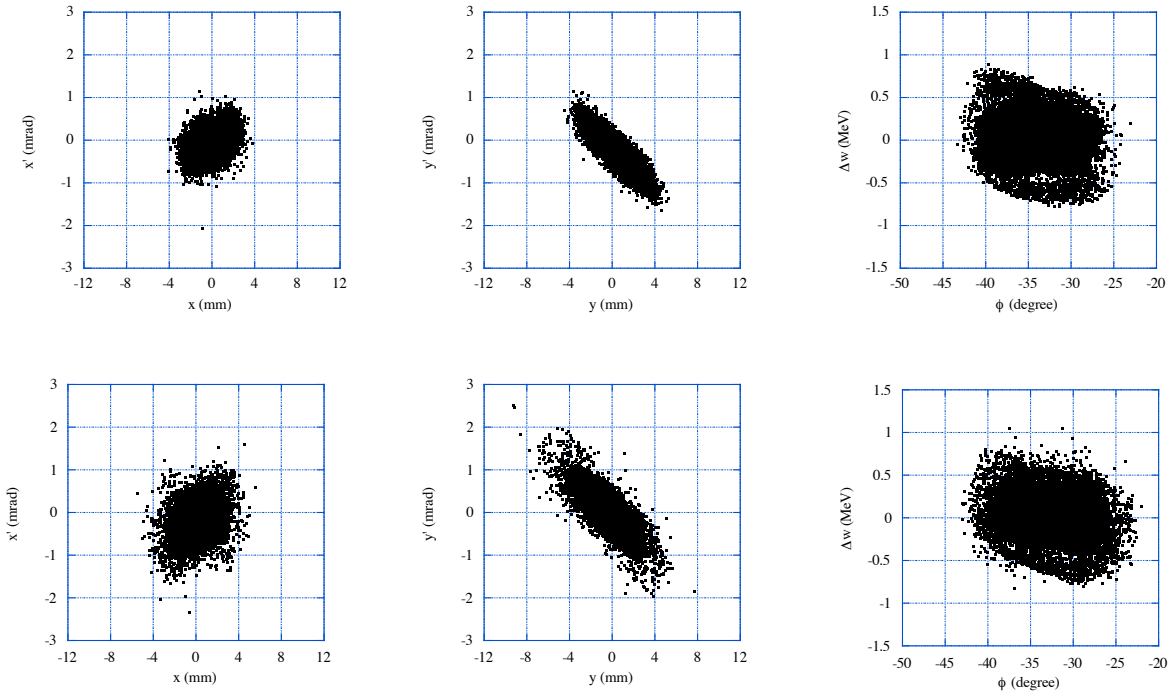

Fig. 2.1.4.3.1 Output emittances for type-1 (upper) and type-3 (lower) simulations.

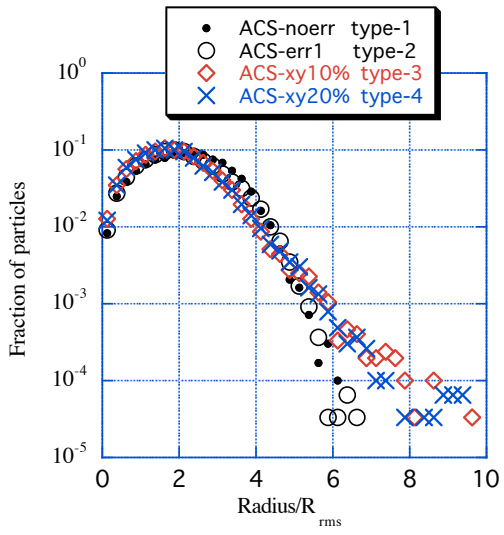

Fig. 2.1.4.3.2 Fraction of the output particles in x-y space as a function of the normalized radius. The output particles were sorted by circular bands having a width of $R_{rms}/8$.

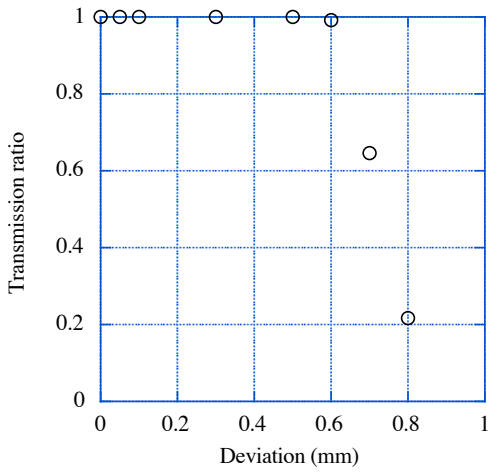

Fig. 2.1.4.3.3 Transmission ratio as a function of random errors in the transverse position of the ACS focusing magnets for the type-5 simulation.

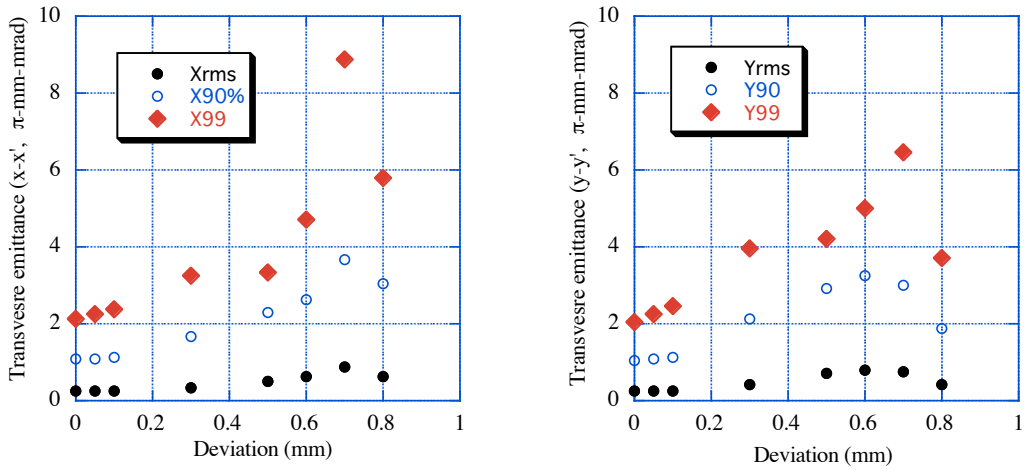

Fig. 2.1.4.3.4 Transverse emittances (rms, 90% and 99%, normalized) as a function of random errors in the transverse position of the ACS focusing magnets (type-5).

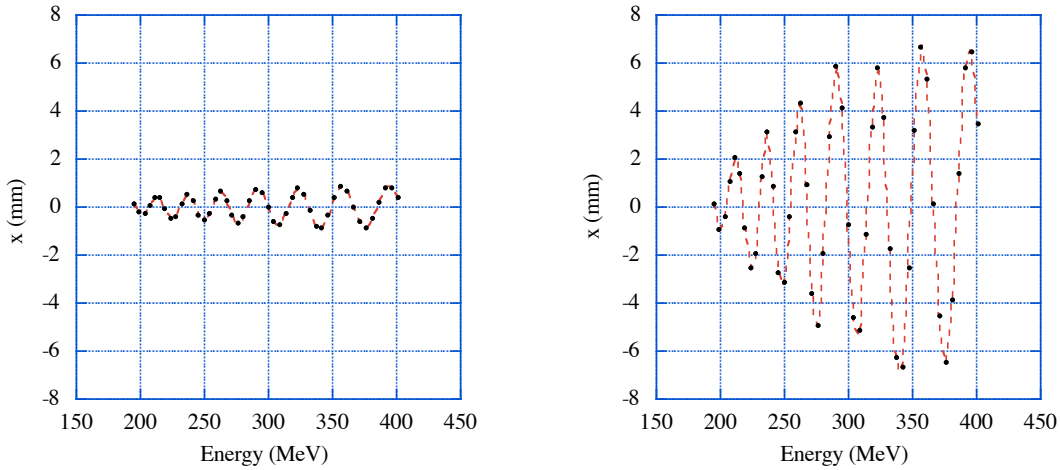

Fig. 2.1.4.3.5 Average x-position of the beam along the ACS for random errors in the transverse position of the ACS focusing magnets of 0.05 mm (left) and 0.5 mm (right).

Results of the LINSAC simulation

Preliminary simulation results with the LINSAC code for acceleration from the DTL to ACS are presented. The same accelerating parameters as the previous one were used. The number of macro-particles was limited to 9000, since part of the extended version using MPI (message-Passing Interface) is under construction. No errors in the fields and alignment were introduced. Figures 2.1.4.3.6 show the emittance variation along the linac. Here, the simulations in the beam-transport lines between the different types of rf structures were performed by the matrix transformation method instead of the beam-transport version of the LINSAC code. Figures 2.1.4.3.7 show the output emittances from the ACS.

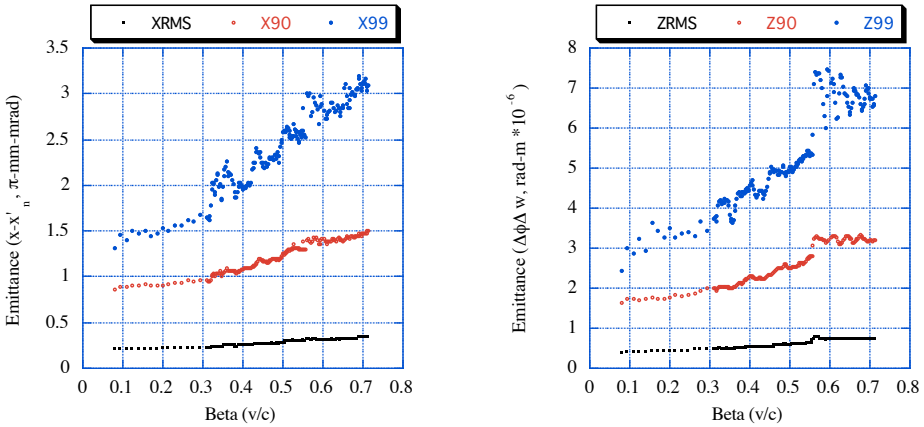

Fig. 2.1.4.3.6 Preliminary results of both transverse (left) and longitudinal (right) emittance variations along the linac calculated with the LINSAC code.

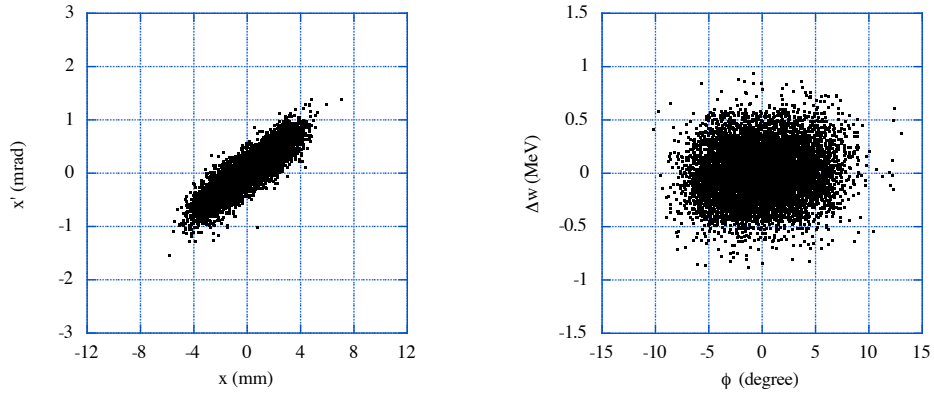

Fig. 2.1.4.3.7 Output emittances from the ACS calculated with the LINSAC code.

Summary of the output beam parameters

The results with the LINSAC code are preliminary, since the number of macro-particles was not sufficiently large and some effects due to the beam-transport lines are observed. Thus, we take the results of type-2 simulation as the standard output beam parameters. They are summarized in Table 2.1.4.3.2.

Table 2.1.4.3.2 Output beam parameters of the 400-MeV linac.

	x-x' π-mm-mrad		y-y' π -mm-mrad		Δϕ–Δw π -MeV-deg	
	rms	99.9%	rms	99.9%	rms	99.9%
Input at 3 MeV	0.200	1.44	0.198	1.43	0.140	1.00
400 MeV output	0.242	3.80	0.242	3.49	0.672	10.9
rms energy width	0.213 MeV					
90% full energy width	0.695 MeV					
99% full energy width	1.31 MeV					